The di-interstitial in graphite

2008 J. Phys.: Condens. Matter 20 395220

(http://iopscience.iop.org/0953-8984/20/39/395220)

J. Phys.: Condens. Matter **20** (2008) 395220 (8pp) doi:10.1088/0953-8984/20/39/395220

The di-interstitial in graphite

C D Latham[1], M I Heggie[1], J A Gámez[2], I Suárez-Martínez[3], C P Ewels[3] and P R Briddon[4]

[1] Department of Chemistry, University of Sussex, Falmer, Brighton BN1 9QJ, UK
[2] Departamento de Química C-IX, Universidad Autónoma de Madrid, Cantoblanco, 28049 Madrid, Spain
[3] Institut des Matériaux Jean Rouxel (IMN/CNRS), 2 Rue de la Houssiniére, BP 32229, F-44322 Nantes, France
[4] Physics Centre, School of Natural Science, University of Newcastle upon Tyne, Newcastle NE1 7RU, UK

Received 9 July 2008, in final form 10 July 2008
Published 4 September 2008
Online at stacks.iop.org/JPhysCM/20/395220

Abstract
Di-interstitial defects appear to play a key role in the microscopic understanding of radiation-induced damage in graphite. Their formation has been invoked as both one of the main causes of dimensional change and as an energy releasing step in annealing cryogenic radiation-induced damage. In the present work, first principles calculations are employed to examine several models for these defects. Two of the structures possess nearly equal energy, yet take very different forms. The results suggest that di-interstitial defects cannot play the principal role in radiation damage that has been assigned to them. The possibility that one of the structures may exhibit ferromagnetism is also investigated.

(Some figures in this article are in colour only in the electronic version)

1. Introduction

Graphite, by virtue of its low cross-section for neutron capture and a reasonable scattering cross-section, is widely used as a reflector and moderator in nuclear reactors. Moderation is the process whereby fast neutrons evolved by nuclear fission are slowed down in order to improve their capture cross-section in the nuclear chain reaction. This is achieved by collisions between neutrons and carbon nuclei. Neutrons can transfer a large proportion of their energy to the carbon atoms when colliding with graphite [1]. This displaces atoms from their normal lattice sites, creating pairs of vacancies and interstitials (Frenkel pairs). In the process, modifications to the properties of the graphite occur, such as dimensional changes, storage of energy (Wigner energy) and variations in its electrical and thermal conductivity [2]. This must be understood in order that the structural and thermal stability of graphite components can be guaranteed.

In this work the role which the di-interstitial system I_2 plays in these phenomena is examined. First principles calculations are employed to model different configurations for the defect, investigate how these might cause dimensional changes, and how they contribute to the Wigner energy.

Graphite possesses a layered structure that can be stacked in three different high-symmetry ways. These are labelled AA, AB, and ABC graphite according to the different relative translations of the layers. The AB form is by far the most abundant [3] and AA is unstable. X-ray crystallography of AB graphite finds hexagonal lattice parameters of $a = 2.4612 \pm 0.0001$ Å, and $c = 6.7079 \pm 0.0007$ Å [4]. Hence, the interlayer distance, d_{002}, is 3.3540 Å, and in-plane bond length is 1.4210 Å, which corresponds to bond order between single (≈1.54 Å) and double (≈1.34 Å) character.

1.1. Radiation-induced damage in graphite

Dimensional changes were the earliest and most obvious observations of irradiated graphite [5]. When it is irradiated with a neutron flux (and generally with any energetic particle), graphite suffers a slight contraction of the basal dimensions and a substantial expansion along the c-direction, both of the changes being dependent on temperature.

A carbon atom needs an energy of $\gtrsim$30 eV to be displaced irreversibly from the lattice [2, 6]. In the ^{235}U fission process, neutrons are produced and released with an average energy of 2 MeV [7]. When an incoming neutron strikes deep in a graphite crystal, it imparts typically 50 keV energy to the primary knock-on atom (PKA), which then initiates a dense cascade of secondary collisions. The energy is dispersed during the ensuing chaos, leaving in its wake all

manner of metastable defects; for example, see [8]. These include intimate Frenkel pairs, i.e. vacancy-interstitial pairs which do not have sufficient energy to separate, and Stone–Wales defects, where two atoms rotate about their mutual bond centre and snap into a metastable state. Theoretical evidence for the former and their role in Wigner energy was provided by the same methods as used in this work [9], and experimental evidence was subsequently provided by electron microscopy [10].

Macroscopic dimensional changes occurring upon irradiation are most clearly seen in good quality graphite (highly oriented pyrolytic graphite). In the c-direction the expansion comprises two parts: an increase in the interlayer spacing, d_{002}, as measured by x-ray, neutron, or electron diffraction and an increase in the number of layers. From early on, irradiation-induced changes observed by small angle cold neutron scattering experiments were linked to increases in d_{002}, and were interpreted in terms of a homogeneous distribution of small clusters of interstitials (I_n, $n = 4 \pm 2$) [11].

The received wisdom for the cause of changes in the effective number of graphene layers is interstitial aggregation giving rise to prismatic dislocation loops (the 'plating out' process). After high-temperature irradiation or high-temperature annealing, such loops can be large and clearly visible in weak beam transmission electron microscopy (TEM) [12].

In apparent conflict with this wisdom, it has long been recognized that if small I_n clusters were to exist, then they could not be nuclei for prismatic dislocation loops, because this would contradict the known kinetics of loop formation [13].

The putative role of I_2 has been modelled by Niwase [14], yielding apparent agreement with experiment by dint of deducing properties and concentrations for I_2 from the fit to experiment.

In the early experiments of irradiation on graphite it was observed that graphite stores energy in its structure and that this energy can later be released by annealing, i.e. thermal activation [15]. Significant energy storage is found for all radiation temperatures from 0 K to approximately 500 K. As a rule of thumb, graphite irradiated at one temperature will begin releasing substantial energy from 50 K above this temperature at normal annealing temperature ramp rates.

In a simple model, this release could be associated with interstitial aggregation or by annihilation with vacancies, provided the interstitial had a low energy of migration. Until recently the easy migration of the interstitial was the prevailing belief, and energy release at low temperature, e.g. 100 K, was associated with processes such as dimerization, and consequent c-axis expansion [16]. At higher annealing temperatures there is a pronounced energy release peak near 475 K, whose origin was suggested by Iwata [17] to be due to the annihilation of I_2 with two vacancies. Thus, according to this picture, I_2 predominates at room temperature [14]. However, some weaknesses in this model have been exposed—notably that the isolated interstitial I has a migration barrier of 1.4 eV [18]—and other authors suggest alternative explanations. For example, Ewels *et al* attribute the 475 K peak to the recombination of intimate Frenkel pairs [9].

1.2. Method

The total energies E_{total} of supercells are calculated using a method based on self-consistent local-density-functional theory, AIMPRO. Only a summary of the main points is provided here. For a more detailed description see [19–21].

The exchange–correlation energy contribution is evaluated according the formula described by Perdew and Wang [22]. A basis set of Cartesian Gaussian orbitals is used to describe the Kohn–Sham wavefunctions of the valence electrons. Suitable multiplicative factors provide s-, p-, and optionally for each exponent, d-orbital symmetries. Basis sets are generated and optimized for hexagonal AB graphite by the procedure in [20]. Carbon atoms are described using four exponents each, where d functions are applied to only the second smallest exponent ($pdpp$). They retain full variational freedom within the AIMPRO formalism and are *not* contracted (an option which is available). Core electrons are replaced by norm-conserving pseudopotentials based on the Hartwigsen–Goedecker–Hutter (HGH) scheme [23]. The charge density is represented by a plane-wave basis in reciprocal space. An automatic procedure ensures that the number of shells of vectors $\boldsymbol{R}_L$ used to evaluate the Madelung energy is sufficient. The kinetic energy cutoff E_{cut} for the charge-density plane-wave basis that is necessary to achieve convergence for E_{total} better than a required level ϵ depends on the pseudopotentials employed. In the present work $E_{\text{cut}} \geqslant 248$ hartrees or about 6.8 keV provides $\epsilon \lesssim 0.1$ meV/atom.

The forces acting on each atom are given by an analytical formula derived from the total energy expression. Structural optimization to minimize the total energy is performed by a conjugate-gradient algorithm. This halts when the change in total energy on successive iterations is $\Delta E_{\text{total}} \lesssim 0.3$ meV. Model defects are constructed in supercells of various sizes with either hexagonal or orthorhombic crystal symmetry. The lattice parameters describing these supercells that minimize E_{total} for pure graphite are found to be $a = 2.446$ and $c = 6.519$ Å, which are close to the observed values.

The Monkhorst–Pack (MP) scheme is used to sample the band structure [24]. Both the largest reciprocal lattice vector of the charge-density Fourier expansion, and the mesh of $\boldsymbol{k}$-points are chosen so that the total energy E_{total} is converged with respect to these parameters ($\epsilon \lesssim 0.1$ meV/atom). The Brillouin zone sampling points are folded into the irreducible set, according to the symmetry of the system. Furthermore, graphite must be treated as a metal; hence, the occupancies of each Kohn–Sham level are filled according to the first-order Methfessel–Paxton scheme [25]. The value of the parameter $k_{\text{B}}T$ used for this scheme has very little effect on the outcome over a range of several orders of magnitude. For the present work it is 0.01 eV.

Formation energies of defects are calculated by the conventional method as described by previous authors [26–30]. For a system containing only one type of atom (i.e. carbon), and where there are no charged defects, this is

$$E_{\text{f}} = E_{\text{d}} - n_{\text{C}}\mu_{\text{C}}, \tag{1}$$

where E_{f} is the formation energy of a defect and E_{d} is the total energy of a supercell containing a defect that is composed

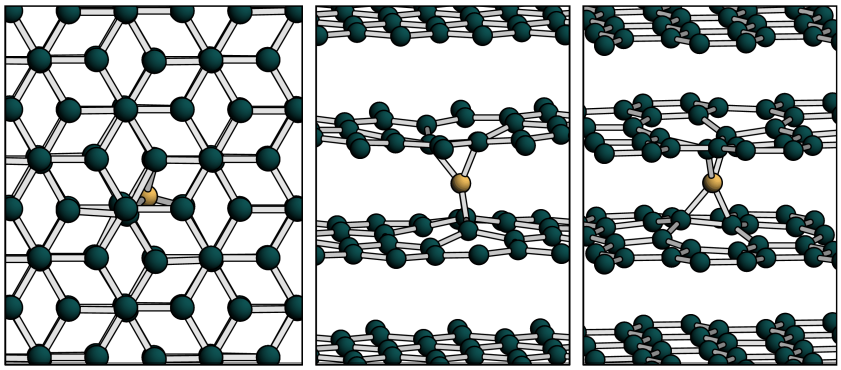

Figure 1. The spiro-interstitial defect is the lowest energy structure for an isolated self-interstitial atom in graphite. Its calculated formation energy is $E_f = 5.85$ eV. The symmetry of this defect is C_2.

from n_C carbon atoms, each having chemical potential μ_C. The chemical potential of carbon atoms is defined to be the Gibbs free energy per particle. For condensed matter at ordinary temperatures and pressures, the entropy and pressure contributions to the Gibbs free energy can be neglected. Hence, μ_C is the total energy per carbon atom in pure, ideal graphite.

2. Results

2.1. Structures

The hexagonal structure of graphite appears simple until defects are introduced. Even knowing that Nature tends to favour higher rather than low-symmetry structures, there are many ways in which interstitial-type defects could conceivably be constructed. Furthermore, the ability of carbon atoms to adopt different hybridization states leads to complex energy surfaces with deep local minima. Consequently, it took many years to establish the structure of the single self-interstitial in graphite [31].

It is also known that the presence of bridging defects can induce basal shear in small models of interstitial-type defects [32]. Preliminary investigations by us, using models based on a $4 \times 4 \times 1$ hexagonal unit cell containing 32 atoms in the ideal structure confirm this picture. This also established that it is necessary to use much larger models, and perform many trials in order to conduct a thorough investigation. Thus, the results reported here are based on models in $4 \times 2 \times 2$ and $6 \times 3 \times 2$ orthorhombic unit cells, which contain 128 and 288 atoms, respectively, in the ideal structure.

Note that only graphitic structures are considered; no amorphous forms are included, meaning that the models do not transform into a disordered configuration. Consideration is also given to optimization of the model structures with constant and variable lattice parameters. With only one exception, basal slip is always inhibited by constraining one atom in each graphene sheet so it may move only along the c-direction. These four atoms also have the same coordinates in the basal directions; hence, they lie in a line along the c-direction. The model defects are constructed such that they are located as far as possible from the four constrained atoms.

2.2. Spiro-interstitial

In order to estimate the energy needed to dissociate di-interstitial defects into two isolated self-interstitial atoms, it is first necessary to find the total energy of a supercell containing a single self-interstitial atom I. Its structure is taken to be that known from previous work, i.e. the spiro-interstitial (figure 1), so called because its five-atom core resembles the carbon skeleton of a spiropentane molecule [32, 33]. This defect has C_2 symmetry. The present work also provides validation of the earlier calculations, since here the supercells used are larger and the convergence criteria are stricter.

The formation energy of I, when basal slip is inhibited, and the lattice parameters held fixed at their calculated values for ideal graphite, is $E_f = 5.85$ eV. *This structure is taken to be the reference state for isolated* I.

When basal slip is allowed, on this occasion only, then the energy of the system—strictly a superlattice of I repeated in $4 \times 2 \times 2$ orthorhombic unit cells—falls by 0.36 eV.

Optimization of the lattice parameters together with the atom coordinates, within the constraint of no basal slip, yields a total energy that is lower by less than 5 meV. There is barely any effect on the lattice parameters, leading to an effective volume per defect of only 0.097 Å^3, nearly all of which is accounted for by expansion in the *basal* directions. The calculated volume per atom in ideal graphite is 8.443 Å^3; hence, the volume per defect is less than 1.2 % of the atomic volume, which is very much smaller than the figure of 3.3 atomic volumes per interstitial deduced by Maeta *et al* [16]. This strongly undermines the assumptions in [14].

2.3. Di-interstitials

Following a process of thorough examination, eight initial model structures, constructed by placing pairs of C atoms separated by ≈1.2–1.6 Å in the central interlayer region of $4 \times 2 \times 2$ supercells, have yielded six distinct metastable bound states for I_2. Four can be classified as bridging structures which join adjacent graphene layers together. In two of these the interstitial C–C pair is oriented at an angle to the basal plane (figures 2 and 3), while for the other two cases the interstitial atoms are both located midway between two

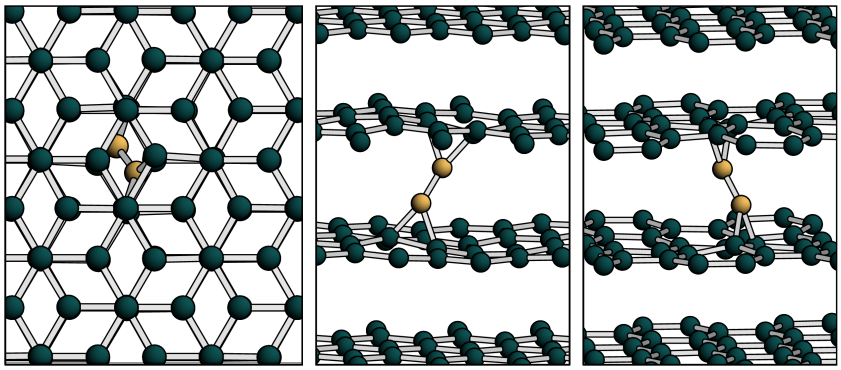

Figure 2. The twin-triangle interlayer bridge defect is the second lowest energy structure for a pair of self-interstitial atoms in graphite. Its calculated binding energy relative to two isolated spiro-interstitial atoms is $E_b \approx 3$ eV. The symmetry of this defect is C_i (or S_2).

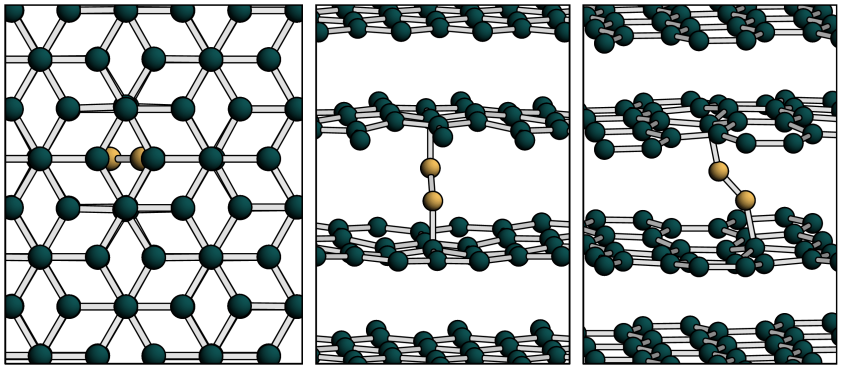

Figure 3. The bent interlayer bridge defect is the third lowest energy structure for a pair of self-interstitial atoms in graphite. Its calculated binding energy relative to two isolated spiro-interstitial atoms is $E_b = 2.4$ eV. The symmetry of this defect is C_{2h}.

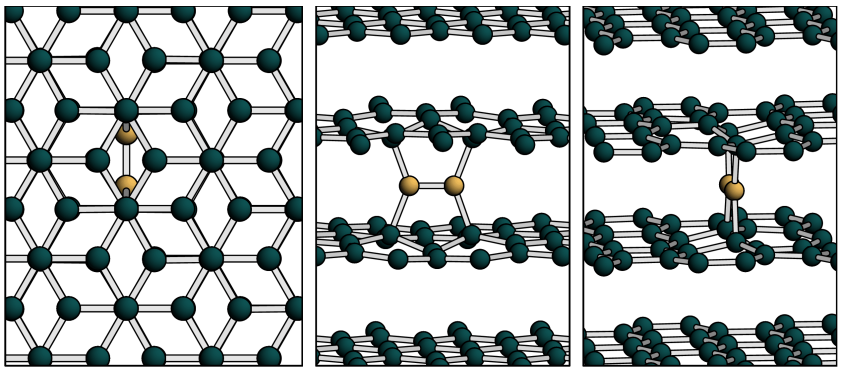

Figure 4. The C–C pair and its four neighbouring atoms in the bi-pentagon interlayer bridge defect shown here lie on a $(10\bar{1}0)$ plane. Its calculated binding energy relative to two isolated spiro-interstitial atoms is $E_b = 2.3$ eV. The symmetry of this defect is C_{2h}.

sheets (figures 4 and 5). It can be seen that one of these defects has C_i symmetry, while the other three have C_{2h} symmetry. A fifth structure, with C_s symmetry, takes the form of a grafted or intralayer bridge where the local bonding arrangement comprises two pentagonal and two heptagonal rings, reminiscent of a Stone–Wales defect (figure 6). The C–C unit is oriented approximately in a $[11\bar{2}0]$ direction, and located over the centre of a hexagonal ring from the original lattice. Finally, the last of the six structures can be described as a split-interstitial pair. It possesses four atoms in a nearly square configuration, giving it C_{2v} symmetry with two equivalent C–C bonds ($\alpha\beta = \alpha'\beta' = 1.511$ Å), and two inequivalent C–C bonds ($\alpha\alpha' = 1.611$ Å, $\beta\beta' = 1.597$ Å), where α and β take their usual meanings in the graphite structure (figure 7). In all the figures, the interstitial atoms are highlighted to identify them. This is more apparent in the electronic version of this document where contrasting colours are used.

All six configurations possess relatively large binding energies E_b relative to two isolated spiro-interstitials, ranging from 1.34 eV for the split-interstitial pair, to about 3 eV for the grafted, intralayer bridge. One of the two interlayer bridging

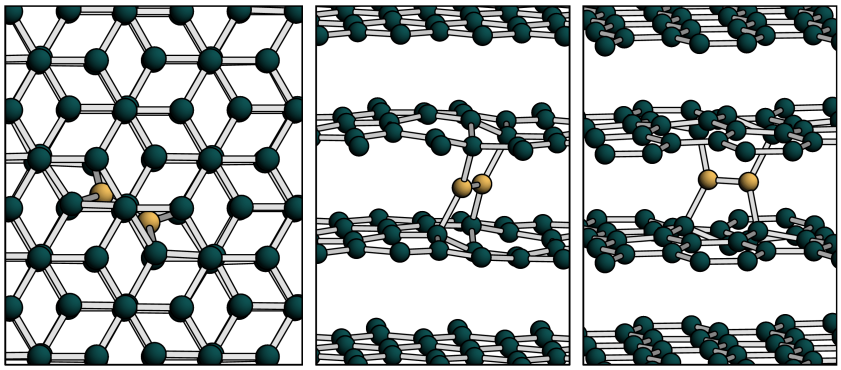

Figure 5. The calculated binding energy for the skew bi-pentagon interlayer bridge defect shown here, relative to two isolated spiro-interstitial atoms, is $E_b = 1.5$ eV. The symmetry of this defect is C_{2h}.

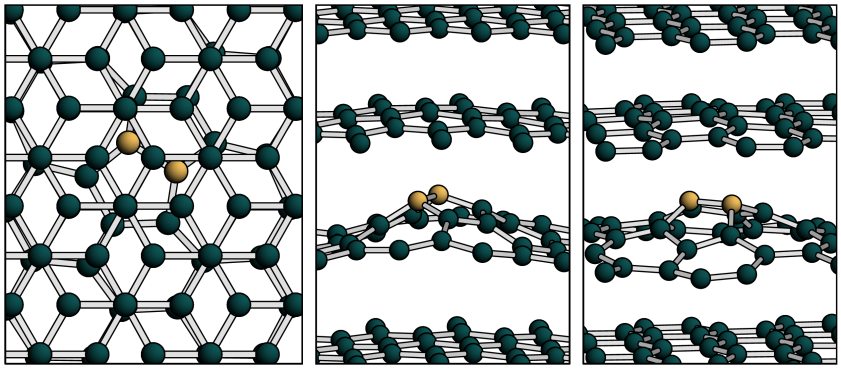

Figure 6. The grafted intralayer bridge defect is the lowest energy structure for a pair of self-interstitial atoms in graphite. Its calculated binding energy relative to two isolated spiro-interstitial atoms is $E_b \approx 3$ eV. The symmetry of this defect is C_s.

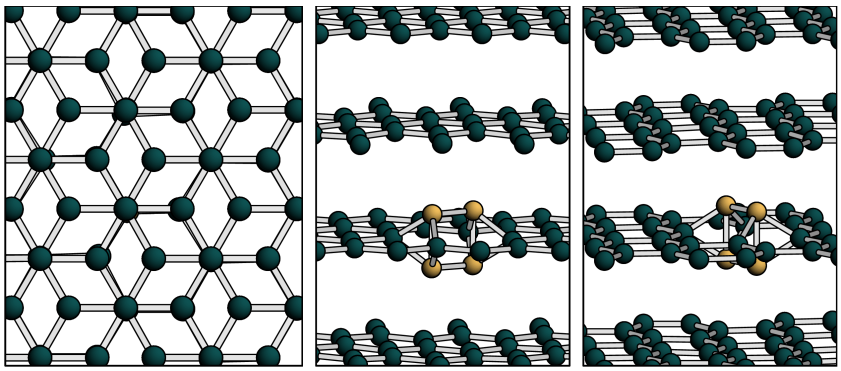

Figure 7. The double split-interstitial defect adopts a nearly square configuration on a $(11\bar{2}0)$ plane. Note that although there are only two additional atoms, the core of the defect possesses two equivalent $\alpha\beta$ C–C pairs. Its calculated binding energy relative to two isolated spiro-interstitial atoms is $E_b = 1.3$ eV. The symmetry of this defect is C_{2v}.

defects, where the C–C pair is oriented at an angle to the basal plane, also has a binding energy that is slightly more than 3 eV relative to two Is; the other has $E_b = 2.40$ eV. In the first case, each interstitial atom is bonded to two host atoms from the neighbouring graphene sheet, while in the second case each interstitial atom is bonded to only one host atom. Thus, the first has a twin-triangle structure, and the other forms a bent bridge.

The twin-triangle interlayer bridge is also the end point for three of the eight initial trial configurations following optimization of the total energy. In one of these three trials the two host C–C bonds nearest to the interstitial atoms are deliberately opened to about 2.3 Å in the initial structure to test whether the final, closed form is a local minimum in energy relative to the open form. It is not: the two host atoms at the base of each triangle are separated by about 1.55 Å in the optimized structure, similar to the C–C distance in diamond. The inner C–C bond is about 1.29 Å long, suggesting that it has double bond character, while the two inequivalent interstitial-host bond lengths are about 1.44 and 1.46 Å long, which is slightly larger than the in-plane C–C distance of graphite (calculated to be 1.41 Å).

Table 1. Properties of interstitial defects in graphite calculated using 4 × 2 × 2 supercells. E_f is the formation energy as defined by equation (1). E_b is the binding energy of di-interstitial defects with respect to two isolated spiro-interstitial atoms using fixed lattice parameters. C–C is the distance between the pair of interstitial C atoms. V is the effective volume per defect when the lattice parameters and atom positions are both optimized; Δa and Δc are the fractional expansion in the a and c lattice parameters that the defects induce. ΔE is the energy associated with the expansion.

Description	E_f (eV)	E_b (eV)	C–C (Å)	V (Å^3)	Δa (%)	Δc (%)	ΔE (eV)
Single spiro I[a]	5.85	0.00	∞	0.10	+0.07	+0.00	−0.00
Twin-triangle	8.63	3.07	1.291	3.00	+0.14	+4.15	−0.31
Bent bridge	9.31	2.40	1.211	2.95	+0.05	+4.26	−0.87
Bi-pentagon	9.39	2.32	1.348	0.99	+0.10	+1.25	−0.05
Skew bi-pentagon	10.23	1.47	1.345	0.60	+0.01	+0.88	−0.02
Grafted, intralayer	8.92	2.78	1.402	3.33	+0.25	+4.41	−0.44
Split pair	10.36	1.34	1.511	0.95	−0.04	+1.49	−0.05

[a] N.B. The data for I are for one, isolated self-interstitial atom.

The two interlayer bridge structures, where the interstitial atoms both lie midway between two neighbouring graphene sheets, adopt a bi-pentagon arrangement. In one case the interstitial C–C pair and the four other atoms that they are bonded to lie in a $(10\bar{1}0)$ plane (figure 4); in the other case they take a skewed configuration (figure 5). The binding energies of these two bi-pentagon structures are $E_b = 2.32$ eV and $E_b = 1.47$ eV for the 'straight' and 'skewed' forms, respectively.

Estimates for the effective volume per defect are hampered by problems with achieving self-consistent total energies during simultaneous optimization of both the lattice parameters and atom coordinates. Nevertheless, the results for nearly complete energy minimization can be reported here. These are shown in table 1, together with other data.

Since the supercells have orthogonal lattice vectors, the hexagonal crystal symmetry is broken, and hence the relaxation in the basal directions is anisotropic. Thus, the a lattice parameter for each optimized supercell is deduced from the area of its basal plane using the relation $a = \sqrt{(a'b'/\sqrt{3})}$, where a' and b' represent the two lattice parameters of the orthorhombic supercell in the basal plane.

Notice that the two lowest energy di-interstitial defects have effective volumes ≈3 Å^3, i.e. less than 35% of an atomic volume. Most of the expansion that they induce is in the c-direction; however, at under 5%, this is much smaller than the amount observed in moderately irradiated graphite (e.g. ∼10^{26} m^{-2} neutrons [4]). Furthermore, they induce a slight *expansion* in the basal directions, contrary to the contraction which occurs. This further undermines the conclusions of Maeta *et al* [16] and Niwase [14], where it is assumed that the volume per interstitial decreases slightly upon formation of I_2.

The above results are for model defects in 4 × 2 × 2 supercells where distortions of the underlying graphite structure are localized around the interstitial atoms and their immediate neighbours. However, it is clear upon inspection that the grafted intralayer bridge requires a larger supercell to accommodate it properly: its structure is artificially constrained by the finite size of the model, particularly in the basal directions. Thus, the twin-triangle interlayer bridge has a binding energy $E_b = 3.07$ eV in a 4 × 2 × 2 supercell, which is 0.29 eV larger than the intralayer bridge, while in the 6 × 3 × 2 supercell E_b is 0.11 eV smaller.

Table 2. Properties of model defects calculated using 6 × 3 × 2 supercells. The quantities E_f, E_b and C–C are as defined previously for table 1.

Description	E_f (eV)	E_b (eV)	C–C (Å)
Single spiro I	5.88	0.00	∞
Twin-triangle	8.74	3.02	1.291
Grafted, intralayer	8.63	3.13	1.396
Isolated pentagon	10.99	0.77	1.428

In other words, using a larger supercell makes E_f 0.29 eV smaller for the intralayer defect, while making it 0.11 eV larger for the twin-triangle defect. This can be interpreted as validating the smaller supercell model for the twin-triangle bridge—since its formation energy is not significantly smaller in the larger supercell—while confirming the suspicion that the smaller supercell is inadequate for the grafted intralayer bridge, owing to the relatively large decrease in energy which is found. Furthermore, $E_f = 8.75$ eV for one of the three trial configurations in the smaller supercell giving a twin-triangle bridge at the end of the optimization procedure. Thus, it is reasonable to conclude that for this defect E_f is essentially the same for both sizes of supercell, within the accuracy of the method. Inspection of the coordinates of the four atoms which are constrained to block slip provides an indication of whether the 6 × 3 × 2 supercell (with fixed lattice parameters) is sufficiently large for the grafted intralayer bridge model. The largest displacement in the c-direction (taking into account a small net translation of the centre of mass of the host atoms ≈0.002 Å) for the larger supercell is less than 0.09 Å, while for the smaller 4 × 2 × 2 one it is about four times greater at 0.37 Å.

It can be seen that in the 6 × 3 × 2 supercell, the grafted intralayer defect can be rearranged by a 90° Stone–Wales rotation of one of its heptagon–hexagon bonds to yield a new structure. This transforms one of the pentagons into a hexagon and the neighbouring hexagon into a pentagon, leaving two isolated pentagons, separated by the new hexagon—see figure 8. The defect has no identifiable symmetry. Although this isolated pentagon defect bears some similarity to its parent, the total energy is 2.36 eV higher.

A summary of the main results for the larger supercell models is provided in table 2.

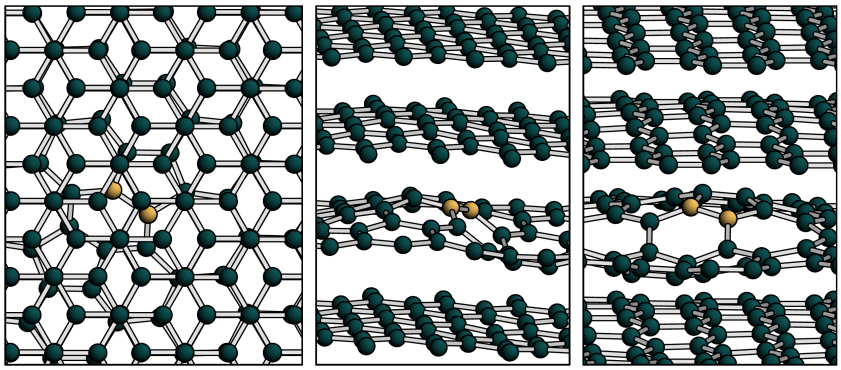

Figure 8. The isolated pentagon defect is obtained by a rearrangement of the grafted intralayer bridge. Its calculated binding energy relative to two isolated spiro-interstitial atoms is $E_b = 0.8$ eV. No symmetry can be identified for this defect.

Table 3. Spin-polarized relative energies $E(N)$ of a bi-pentagon interlayer bridge with N unpaired electrons with respect to the non-spin-polarized defect.

N	$E(N)$ (eV)
0	0.000
1	0.015
2	0.034

2.4. Magnetism

Graphite exhibits a large diamagnetic susceptibility which is affected by the degree of crystalline order, and the presence of defects [34, 35]. The phenomenon is of sufficiently large magnitude to be exploited in the form of magnetic levitation toys using small pieces of highly oriented pyrolytic carbon and strong permanent magnets.

Under certain circumstances, ferromagnetism appears to be observed in graphitic materials [36, 37]. It is suggested that the presence of sp^3-hybridized carbon atoms in these materials may be responsible for their magnetic properties; however, theoretical studies have directed their attention to vacancy-type defects [38–40]. Thus, it is natural to ask whether any of the interstitial defects considered here might possess a nonzero magnetic moment.

Inspection of the bi-pentagon interlayer bridge reveals that it is potentially a magnetic defect. Its local structure comprises two linked fivefold rings with four single bonds from the host to the I_2. Hence, the four host atoms which are bonded to the I_2 are sp^3 hybridized. They are also next nearest neighbours to each other, raising the possibility that the intervening host atoms may each have an unpaired electron in their p_z orbitals. However, according to spin-polarized calculations, the ground state is nonmagnetic: the total energy of the system is lowest when $S = 0$. See table 3.

The fact that local spin density approximation tends to overstabilize high spin states increases the likelihood that this conclusion is correct and not an artefact of the method. Nevertheless, this result does not exclude the possibility that other, related structures with sp^3-hybridized carbon atoms in graphitic materials could carry a nonzero magnetic moment. It shows, in fact, the general form that suitable defects might take. Extended defects, such as reconstructed dislocations, where the local structure contains sp^3-hybridized carbon atoms, could also exhibit ferromagnetism.

3. Summary and conclusions

The conventional model for radiation-induced dimensional change in graphite, involving aggregation of interstitial atoms into new layers at the expense of existing ones, now appears to be untenable. Onset of dimensional change occurs at temperatures well below that where interstitials would become mobile. Then, as shown by this work, the first stage of interstitial aggregation leads to di-interstitial states which are strongly bound, immobile defects, and induce dimensional changes inconsistent with the measured values. With binding energies of more than 3 eV, the two lowest energy forms of di-interstitial defect will not decompose or migrate easily. Thus, the decomposition of I_2, followed by migration of I, and subsequent aggregation into larger interstitial clusters, as required by the conventional model to explain the origin of Wigner energy in the low-temperature regime, must be incorrect. The calculations also show that the volume per defect for I and I_2 is much smaller than that assumed for the conventional model in the high-temperature regime.

Shear of the layers in the basal directions will, in general, lower further the energies of bridging defects, such as those considered here. Since basal dislocations are a common feature in graphite—and these have locally sheared regions—bridging defects are likely to be associated with them. Basal dislocations in turn can induce buckling of the layers in graphite, and this can account for the observed radiation-induced dimensional change [41, 42]. Moreover, the interstitial defects themselves all induce local, small-scale buckling of the layers. The distortion is particularly large for the grafted intralayer bridge.

Acknowledgments

The authors wish to thank British Energy Generation Limited for providing financial support. CDL also thanks the NorPRINS collaboration for funding travel expenses. The views expressed in this work are independent from those which may be held by our sponsors.

References

[1] Marsden B J 1996 Irradiation damage in graphite *Tech. Rep.* TECDOC-901 IAEA, Vienna (available at http://www.iaea.org/inisnkm/nkm/aws/htgr/abstracts/abst_28008802.html)
[2] Kelly B T 1981 *Physics of Graphite* (Essex: Applied Science Publishers)
[3] Ubbelohde A R and Lewis F A 1960 *Graphite and its Crystal Compounds* (Oxford: Clarendon)
[4] Kelly B T 2000 Irradiation damage in graphite due to fast neutrons in fission and fusion systems *Tech. Rep.* TECDOC-1154 IAEA, Vienna (available at http://www.iaea.org/inisnkm/nkm/aws/htgr/abstracts/abst_xa54410.html)
[5] Walker P L (ed) 1966 *Chemistry and Physics of Carbon* vol 2 (London: Edward Arnold)
[6] Banhart F 1999 *Rep. Prog. Phys.* **62** 1181–221
[7] Neighbour G B J 2000 *J. Phys. D: Appl. Phys.* **33** 2966–72
[8] Pregler S K, Hayakawa T, Yasumatsu H, Kondow T and Sinnott S B 2007 *Nucl. Instrum. Methods* B **262** 240–8
[9] Ewels C P, Telling R H, El-Barbary A A, Heggie M I and Briddon P R 2003 *Phys. Rev. Lett.* **91** 025505
[10] Urita K, Suenaga K, Sugai T, Shinohara H and Iijima S 2005 *Phys. Rev. Lett.* **94** 155502
[11] Martin D G and Henson R W 1967 *Carbon* **5** 313
[12] Amelinckx S and Delavignette P 1960 *Phys. Rev. Lett.* **5** 50–1
[13] Brown L M, Kelly A and Mayer R M 1969 *Phil. Mag.* **19** 721–41
[14] Niwase K 1995 *Phys. Rev.* B **52** 15785–98 erratum: [43]
[15] Wigner E P 1946 *J. Appl. Phys.* **17** 857–63
[16] Maeta H, Iwata T and Okuda S 1975 *J. Phys. Soc. Japan* **39** 1558–65
[17] Iwata T 1985 *J. Nucl. Mater.* **133/134** 361–4
[18] Li L, Reich S and Robertson J 2005 *Phys. Rev.* B **72** 184109
[19] Briddon P R and Jones R 2000 *Phys. Status Solidi* b **217** 131–71
[20] Goss J P, Shaw M J and Briddon P R 2007 *Marker-Method Calculations for Electrical Levels using Gaussian-Orbital Basis Sets* (*Topics Appl. Phys.* vol 104) (Berlin: Springer) chapter 3, pp 69–94
[21] Rayson M J and Briddon P R 2008 *Comput. Phys. Commun.* **178** 128–34
[22] Perdew J P and Wang Y 1992 *Phys. Rev.* B **45** 13244–9
[23] Hartwigsen C, Goedecker S and Hutter J 1998 *Phys. Rev.* B **58** 3641–62
[24] Monkhorst H J and Pack J D 1976 *Phys. Rev.* B **13** 5188–92
[25] Methfessel M and Paxton A T 1989 *Phys. Rev.* B **40** 3616–21
[26] Zhang S B and Northrup J E 1991 *Phys. Rev. Lett.* **67** 2339–42
[27] Northrup J E and Zhang S B 1993 *Phys. Rev.* B **47** 6791–4
[28] Pöykkö S, Puska M J and Nieminen R M 1996 *Phys. Rev.* B **53** 3813–9
[29] Mattila T and Nieminen R M 1996 *Phys. Rev.* B **54** 16676–82
[30] Van de Walle C G, Limpijumnong S and Neugebauer J 2001 *Phys. Rev.* B **63** 245205
[31] Telling R H and Heggie M I 2007 *Nat. Mater.* **87** 4797–846
[32] Telling R H, Ewels C P, El-Barbary A A and Heggie M I 2003 *Nat. Mater.* **2** 333–7
[33] Heggie M I, Eggen B R, Ewels C P, Leary P, Ali S, Jungnickel G, Jones R and Briddon P R 1998 *Fullerenes: Chemistry, Physics, and New Directions* (*Recent Advances in the Chemistry and Physics of Fullerenes and Related Materials* vol 6) ed K M Kadish and R S Ruoff (Pennington, NJ: The Electrochemical Society) pp 61–7
[34] Fischbach D B 1961 *Phys. Rev.* **123** 1613–4
[35] Soule D E and Nezbeda C W 1963 Diamagnetic susceptibility of graphite by the Faraday method *Tech. Rep.* WADD-TR-61-72, vol 39, AF Materials Laboratory Aeronautical Systems Division, Air Force Systems Command, Wright-Patterson Air Force Base, Ohio (available at http://contrails.iit.edu/DigitalCollection/1961/WADDTR61-072volume39.pdf)
[36] Esquinazi P, Spemann D, Höhne R, Setzer A, Han K H and Butz T 2003 *Phys. Rev. Lett.* **91** 227201
[37] Rode A V, Gamaly E G, Christy A G, Fitz Gerald J G, Hyde S T, Elliman R G, Luther-Davies B, Veinger A I, Androulakis J and Giapintzakis J 2004 *Phys. Rev.* B **70** 054407
[38] Lehtinen P O, Foster A S, Ayuela A, Krasheninnikov A, Nordlund K and Nieminen R M 2003 *Phys. Rev. Lett.* **91** 017202
[39] Lehtinen P O, Foster A S, Ma Y, Krasheninnikov A V and Nieminen R M 2004 *Phys. Rev. Lett.* **93** 187202
[40] Faccio R, Pardo H, Denis P A, Yoshikawa Oeiras R, Araújo-Moreira F M, Veríssimo-Alves M and Mombrú A W 2008 *Phys. Rev.* B **77** 035416
[41] Heggie M I, Suárez-Martínez I, Haffenden G, Savini G, El-Barbary A, Ewels C, Telling R and Cousins C S G 2007 *Management of Ageing in Graphite Reactor Cores* vol 309, ed G B Neighbour (Cambridge: The Royal Society of Chemistry) pp 83–90
[42] Heggie M I, Suárez-Martínez I, Davidson C R, Savini G, Haffenden G and Campenera J M 2008 Buckle, ruck, and tuck: the manipulation of graphite sheets, in preparation
[43] Niwase K 1997 *Phys. Rev.* B **56** 5685